Power of the wingbeat: modelling the effects of flapping wings in vertebrate flight

M. Klein Heerenbrink, L. C. Johansson, A. Hedenström

Address: Dept. of Biology, Lund University, Sölvegatan 37, SE-223 62 Lund, Sweden

Author for correspondence: Marco Klein Heerenbrink,
e-mail: Marco.Klein_Heerenbrink@biol.lu.se

Abstract

Animal flight performance has been studied using models developed for man made aircraft. For an aeroplane with fixed wings the energetic cost as a function of flight speed can be expressed in terms of weight, wing span, wing area and body area, where more details are included in proportionality coefficients. Flying animals flap their wings to produce thrust. Adopting the fixed wing flight model implicitly incorporates the effects of wing flapping in the coefficients. However, in practice these effects have been ignored.

In this paper the effects of reciprocating wing motion on the coefficients of the fixed wing aerodynamic power model for forward flight are explicitly formulated in terms of thrust requirement, wingbeat frequency and stroke-plane angle, for optimized wingbeat amplitudes. The expressions are obtained by simulating flights over a large parameter range using an optimal vortex wake method combined with a low level blade element method.

The results imply that previously assumed acceptable values for the induced power factor might be strongly underestimated. The results also show the dependence of profile power on wing kinematics. The expressions introduced in this paper can be used to significantly improve animal flight models.

1   Introduction

In the past animal flight performance has been studied in various ways, often borrowing basic principles used in the design and operation of aeroplanes and helicopters. To a large extent this will result in good approximations, as much of the physics is very similar. However, aeroplanes use separated systems for propulsion and lift production, which results in a model for energy use that is relatively simple. Helicopters use a mechanism that combines lift and thrust production, which is more similar to flying animals, but animals use reciprocating wings, rather than rotating wings. This adds another level of complexity, where besides the wingbeat frequency also the wingbeat amplitude is of importance for optimisation. The current work involves a theoretical study on the effects of wingbeat frequency, amplitude and stroke-plane angle, on the aerodynamic efficiency of animal flapping flight. In addition to providing an accurate aerodynamic characterisation of self-powered animal flight, the utility of models like the one presented here is fundamental to understand adaptive flight behaviours in wild animals, ranging from display, foraging, food transport and migration[1]. For example, the power-speed relationship predicts alternative 'optimal' flight speeds that should be selected depending on the ecological context, and observations support the notion that birds and bats are capable of selecting an appropriate context-related flight speed in broad agreement with predictions[2, 3].

Aerodynamic power is commonly separated into components with different underlying mechanisms:

$$P_{\text{aero}} = P_{\text{ind}} + P_{\text{pro}} + P_{\text{body}}, \tag{1}$$

following the practice for aeroplanes[4]. Induced power, P_{ind}, is due to the active acceleration of mass flow in order to produce a force opposing weight and drag (for fixed wing aircraft, the induced power due to thrust production is considered separately as part of engine efficiency). Profile power

P_{pro} is due to the local drag on the wings, and body power P_{body} due to drag on the body. In 1968 Pennycuick applied this model to estimate flight performance in birds[5]. An actuator disk model was used to obtain induced power, while blade-element theory, using quasi-steady aerofoil properties, was used to compute profile power. The energetic model was then expressed in terms of weight, wingspan, body frontal area, air density and air speed as a general model for bird and bat flight. For each component there is a modifying factor, which includes all effects not accounted for by these measurable variables. These factors have been adjusted over the years following field observations of flight speeds [6, 7] and wind tunnel experiments [8]. The effects of wing kinematics should thus be implicitly incorporated in these correction factors. However, little effort has gone into systematically quantifying the effects of reciprocating wings.

The effects of wing kinematics have been studied before and several alternative flight models have been developed. The flapping wings are simulated at different levels of detail. A blade-element approach, similar to [5], was used by Parslew and Crowther [9] to optimize wing kinematics of a pigeon for minimal power. Rayner[10] used a continuous vortex lifting line model for forward flight, accounting for unsteadiness due to flapping and wake deformation. Phlips et al.[11] used a similar lifting line model, but with an active down-stroke and an inactive up-stroke. Hall and Hall[12] developed a method involving a sheet of continuously varying vorticity shed from the flapping wings. This generalized vortex wake method allows for a continuous transition between wake topologies, resembling those observed in wind tunnel studies on birds[13]. The output of the Hall and Hall model is the ideal distribution of circulation over the shed wake for minimum power for a prescribed cyclic wake geometry. This ideal circulation distribution relates to the ideal lift distribution over the wing, which for steady planar wings is the familiar elliptical distribution [14]. Salehipour and Willis [15] used this vortex wake method to investigate an extended parameter space for animal flight, varying reduced frequency, stroke amplitude, thrust and lift. They found that wingbeat kinematics, specifically amplitude and frequency, could be optimized for minimum power. These studies all show that wing kinematics affect the power requirements for flight.

The aim of the current work is to formulate explicit expressions that describe the effects of flapping wings on the different components of aerodynamic power in forward flight (equation 1). These expressions are generally applicable to flying vertebrates, i.e. birds and bats, that use a span reduction during the upstroke. Using the Hall and Hall model [12] a set of solutions was produced for different combinations of thrust ratio, reduced frequencies and stroke-plane angles, where the wingbeat amplitude was optimized for minimum induced power (Section 2). We then used non-linear regressions to express the effects of wing flapping on the drag and power components as functions of those three parameters (Section 3). Finally the expressions are applied to an example to illustrate the implications of the model (Section 4).

2   Wake optimisation

The approach we used for computing aerodynamic power is modified from the Hall and Hall model [12]. In the current section we will first briefly describe the method of finding the optimal circulation distribution for a prescribed wake geometry. This is followed by a description of the wake geometry and how it is optimized.

2.1   Aerodynamic power optimisation for a given geometry

The optimal wake method optimizes the distribution of circulation on a predefined wake geometry, as shown in figure 1. This can be interpreted as a sheet of vortex rings shed at each location the wing passes through the air. The strength (circulation) of each vortex ring is contained in the vector $\mathbf{\Gamma}$. Then an influence matrix $\mathbf{K}_{ind}$ is constructed, describing the induced velocity due to each vortex ring on control points related to all other vortex rings. This matrix is computed using the Biot-Savart law for a unit strength vortex for each ring using the prescribed geometry of the
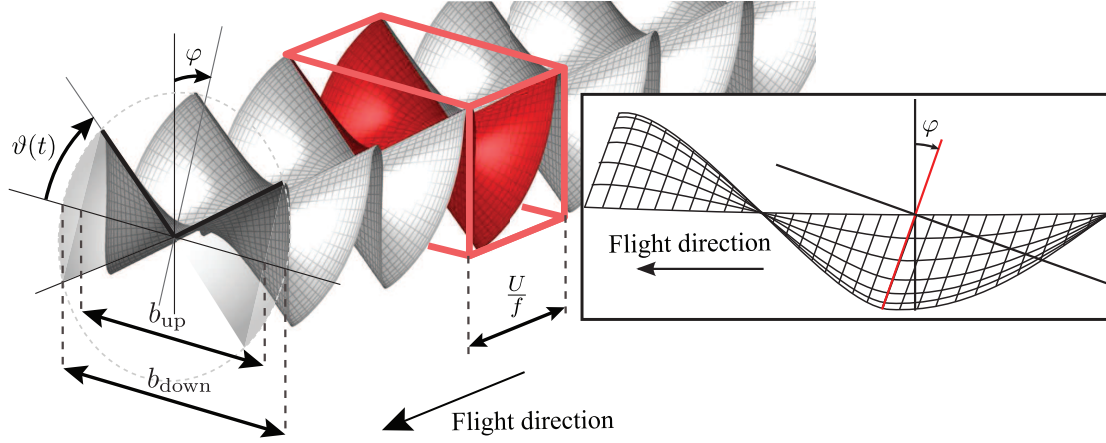
Fig. 1: Definitions describing the wake geometry. Marked selection of the wake mesh is the part that is under consideration for the computation. The other wakes are copies with the same circulation distribution which influence the velocity field of the marked wake. The insert shows a side view, clarifying the definition of the stroke-plane angle φ. The angle $\vartheta(t)$ is within the stroke-plane.

wake:

$$
\mathbf{K}_{\mathrm{ind}} = -\begin{bmatrix}
\mathbf{V}_{1,1} \cdot \mathbf{n}_1 A_1 & \cdots & \mathbf{V}_{1,j} \cdot \mathbf{n}_j A_j & \cdots & \mathbf{V}_{1,N} \cdot \mathbf{n}_N A_N \\
\vdots & & \vdots & & \vdots \\
\mathbf{V}_{i,1} \cdot \mathbf{n}_1 A_1 & \cdots & \mathbf{V}_{i,j} \cdot \mathbf{n}_j A_j & \cdots & \mathbf{V}_{i,N} \cdot \mathbf{n}_N A_N \\
\vdots & & \vdots & & \vdots \\
\mathbf{V}_{N,1} \cdot \mathbf{n}_1 A_1 & \cdots & \mathbf{V}_{N,j} \cdot \mathbf{n}_j A_j & \cdots & \mathbf{V}_{N,N} \cdot \mathbf{n}_N A_N
\end{bmatrix},
$$

where

$$
\begin{aligned}
\mathbf{V}_{i,j} &= \frac{1}{4\pi} \sum_k \frac{\mathbf{r}_{i,j}^{k1} \times \mathbf{r}_{i,j}^{k2}}{|\mathbf{r}_{i,j}^{k1} \times \mathbf{r}_{i,j}^{k2}|} \left(\mathbf{r}_{i,j}^{k0} \cdot \left(\frac{\mathbf{r}_{i,j}^{k1}}{|\mathbf{r}_{i,j}^{k1}|} - \frac{\mathbf{r}_{i,j}^{k2}}{|\mathbf{r}_{i,j}^{k2}|} \right) \right) \ (k \text{ indicates edge of vortex ring } i), \\
\mathbf{r}_{i,j}^{k0} &= \mathbf{x}_i^{k2} - \mathbf{x}_i^{k1} (\text{length of edge } k \text{ of vortex ring } i), \\
\mathbf{r}_{i,j}^{k1} &= \mathbf{x}_j - \mathbf{x}_i^{k1} (\text{distance point } j \text{ to endpoint 1 of edge } k \text{ of vortex ring } i), \\
\mathbf{r}_{i,j}^{k2} &= \mathbf{x}_j - \mathbf{x}_i^{k2} (\text{distance point } j \text{ to endpoint 2 of edge } k \text{ of vortex ring } i).
\end{aligned}
$$

For vortex ring j, $\mathbf{n}_j$ is the normal to the enclosed plane and A_j its area. The velocity contribution of vortex ring i on the control point (centroid) in vortex ring j is indicated by $\mathbf{V}_{i,j}$. For the computation of $\mathbf{K}_{\mathrm{ind}}$ the wake is repeated upstream and downstream of the wake under consideration, representing succeeding and preceding wingbeats. Formally the wake needs to be repeated to infinity both upstream and downstream, but tests for convergence indicated the largest error on the induced power for using only 4 repeated wakes on each side was ~0.5%. With matrix $\mathbf{K}_{\mathrm{ind}}$ the induced power can be computed, $P_{\mathrm{ind}} = \frac{1}{2}\rho f \mathbf{\Gamma}^T \mathbf{K}_{\mathrm{ind}} \mathbf{\Gamma}$, where ρ is the air density and f is the wingbeat frequency. The distribution $\mathbf{\Gamma}$ is still unknown, but it has to satisfy the constraint that the wake should correspond to a prescribed aerodynamic force. This force can be expressed as $\mathbf{F} = \rho f \mathbf{B} \mathbf{\Gamma}$, where the vector $\mathbf{F}$ contains the thrust force T, a side force F_y, and a lift force L. Matrix $\mathbf{B}$ essentially contains the vortex ring area and orientation:

$$
\mathbf{B} = -\begin{bmatrix}
A_1 n_1^x & \cdots & A_j n_j^x & \cdots & A_N n_N^x \\
A_1 n_1^y & \cdots & A_j n_j^y & \cdots & A_N n_N^y \\
A_1 n_1^z & \cdots & A_j n_j^z & \cdots & A_N n_N^z
\end{bmatrix}
$$

Assuming a solution exists for which induced power is minimal, this minimum can be found by finding a vector $\mathbf{\Gamma}$ for which $\partial P_{\mathrm{ind}}/\partial \mathbf{\Gamma} = \mathbf{0}$. As also the force constraint has to be satisfied, the

equation that is minimized is formulated as

$$\Pi = \underbrace{\frac{1}{2}\rho f \boldsymbol{\Gamma}^T \mathbf{K}_{\text{ind}}\boldsymbol{\Gamma}}_{P_{\text{ind}}} + \boldsymbol{\lambda} \cdot \left(\underbrace{\rho f \mathbf{B}\boldsymbol{\Gamma}}_{\mathbf{F}} - \mathbf{F}_R \right),$$

where $\mathbf{F}_R$ is the required force vector to be produced and $\boldsymbol{\lambda}$ is a Lagrange multiplier. By setting the derivatives with respect to $\boldsymbol{\Gamma}$ and $\boldsymbol{\lambda}$ to zero, the solution

$$\begin{pmatrix} \boldsymbol{\Gamma} \\ \boldsymbol{\lambda} \end{pmatrix} = \frac{1}{\rho f} \begin{bmatrix} \mathbf{K}_{\text{ind}} & \mathbf{B}^T \\ \mathbf{B} & \mathbf{0} \end{bmatrix}^{-1} \begin{pmatrix} \mathbf{0} \\ \mathbf{F}_R \end{pmatrix} \tag{2}$$

is found. This solution is specific to the prescribed wake geometry, and therefore dependent on flap angle $\vartheta(t)$, stroke-plane angle φ, the wingspan $b(t)$ and the travelled distance per wingbeat U/f, with U being the flight speed (Figure 1). The ratio between wingspan and travelled distance is found in the reduced frequency $k_f = 2\pi f b/U$, which is therefore a useful parameter to characterize the wake. The solutions for thrust (T) and lift (L) are linearly independent. This means that the solutions can also be characterized by the thrust ratio T/L.

In successive work on the Hall and Hall model [16], the model was extended to include profile drag. Aerofoil viscous drag may be approximated by the equation $d_{\text{vis}} = \frac{1}{2}\rho V^2 c \left(C_{Dv,0} + C_{Dv,2} C_\ell^2 \right)$, where V is the local velocity, c the local chord, $C_{Dv,0}$ the zero lift drag coefficient, $C_{Dv,2}$ the lift dependent drag coefficient and C_ℓ the sectional lift coefficient. This is referred to as viscous drag, as the coefficients are Reynolds number dependent. The lift coefficient can be expressed as $C_\ell = \frac{2\Gamma}{Vc}$, which makes it possible to include the lift dependent viscous drag in equation 2 by extending the influence matrix

$$\mathbf{K}_{\text{vis}} = \mathbf{K}_{\text{ind}} + 4C_{Dv,2}\,\text{diag}\left(\frac{A_j}{c_j}\right), \tag{3}$$

where c_j is the chord length of the wing at the span position corresponding to vortex ring j. By using this formulation lift dependent viscous drag is taken into account during the optimisation of the circulation distribution. The modified circulation distribution also affects the induced power and induced drag, but because this change is due to adding viscous properties it will be counted as lift dependent viscous power, i.e.

$$P_{v,2} = \frac{1}{2}\rho f \boldsymbol{\Gamma}_{\text{vis}}^T \mathbf{K}_{\text{vis}}\boldsymbol{\Gamma}_{\text{vis}} - \frac{1}{2}\rho f \boldsymbol{\Gamma}_{\text{ind}}^T \mathbf{K}_{\text{ind}}\boldsymbol{\Gamma}_{\text{ind}},$$

where $\boldsymbol{\Gamma}_{\text{vis}}$ is the optimal circulation distribution including the viscous model, and $\boldsymbol{\Gamma}_{\text{ind}}$ the solution of the inviscid model.

Several studies have measured the drag of birds [17, 18, 19, 20], bats [21] or their wings [22, 23, 24, 25]. However, few studies have explicitly described the profile drag polar. In the viscous Hall and Hall model [16] a value of $C_{Dv,2} = 0.012$ was taken from empirical measurements on a NACA 4412 aerofoil for a Reynolds number of 6×10^6. This Reynolds number is too high to be representative for animal flight [4]. In the work of Salehipour and Willis [15] values for $C_{Dv,2}$ were estimated based on numerical computations on a NACA 0006 aerofoil. Over a range of Reynolds numbers $10^3 < Re < 10^5$, values varied between 0.01 to 0.05 depending on which angle of attack was chosen for the quadratic fit. In the computations for the current work we use a value $C_{Dv,2} = 0.03$, which is in the middle of the above range (The resulting drag polar also compares well with experimental data from [20]; see ESM S1).

Zero-lift drag is independent of the distribution of circulation and therefore not taken into account in the wake optimisation (equation 2), but its contribution to the power consumption will be estimated from the wake geometry. The zero-lift drag coefficient strongly depends on the local Reynolds number, $Re_c = Vc/\nu$, with ν the kinematic viscosity. The state of the boundary layer, i.e. the position of turbulent transition and possibly separation, will have an effect, but this is ignored in the current work. For an approximation we assume fully laminar attached flow and use Blasius' flat plate boundary layer solution[14, 26]:

$$C_{Dv,0} = \frac{2.66}{\sqrt{Re_c}}. \tag{4}$$

The zero lift drag component of the aerodynamic power is computed as

$$P_{v,0} = \frac{1}{2}\rho f \sum c C_{Dv,0} |\mathbf{V}|^2 A,$$

with $|\mathbf{V}| = \mathrm{d}s/\mathrm{d}t$ representing the geometric speed of the wing section, where $(\mathrm{d}s)^2 = (\mathrm{d}x)^2 + (\mathrm{d}y)^2 + (\mathrm{d}z)^2$.

To complete the viscous model a chord distribution along the wingspan is required. There is a great variety of wing shapes among birds and bats, some having rather rectangular wings, while others have more pointed wings. In the current work we use an elliptical chord distribution

$$\frac{c(y')}{c_{\max}} = \left(1 - 4y'^2\right)^{\frac{1}{2}} \tag{5}$$

where $y' = \frac{y}{b}$ and $c_{\max}$ is the maximum chord such that $b \int_{-1/2}^{1/2} c(y')\, dy' = S$, S being the wing area. It should be noted that this drag model suggests potentially beneficial effects of wing shape depending on the situation, as seen when exposing all the chord dependencies in the viscous drag equation,

$$d_{\mathrm{vis}} = 1.33\rho\sqrt{\nu V^3}\sqrt{c} + 2\rho C_{Dv,2}\Gamma^2\frac{1}{c}. \tag{6}$$

For high tip speeds a pointed tip will decrease zero lift drag, while for high wing tip loadings a broader wing tip will decrease lift dependent drag.

The amount of thrust a bird has to produce for steady flight is, apart from body drag (D_{body}), depending on the drag force on the wing itself, i.e. induced drag and profile drag. These forces are evaluated locally and the components along the flight direction are summed. We compute the local induced drag as the local induced power divided by the local (geometric) velocity, so that

$$D_{\mathrm{ind}} = \frac{1}{2}\rho f \mathbf{\Gamma}^T \mathrm{diag}\left(\frac{1}{|\mathbf{V}|}\frac{\mathrm{d}x}{\mathrm{d}s}\right)\mathbf{K}_{\mathrm{i}}\mathbf{\Gamma}. \tag{7}$$

Similarly, we compute zero lift viscous drag as

$$D_{v,0} = \frac{1}{2}\rho f \sum c C_{Dv,0} |\mathbf{V}|^2 A \left(\frac{1}{|\mathbf{V}|}\frac{\mathrm{d}x}{\mathrm{d}s}\right), \tag{8}$$

and lift dependent viscous drag as

$$D_{v,2} = \frac{1}{2}\rho f \mathbf{\Gamma}_v^T \mathrm{diag}\left(\frac{1}{|\mathbf{V}|}\frac{\mathrm{d}x}{\mathrm{d}s}\right)\mathbf{K}_v\mathbf{\Gamma}_v - D_{\mathrm{ind}}. \tag{9}$$

Thrust required for steady forward flight is the sum of these components, $T = D_{\mathrm{ind}} + D_{v,0} + D_{v,2} + D_{\mathrm{body}}$.

2.2   Optimisation of the wake geometry

The wake geometry represents the shape of the vortex sheet as it separates from the trailing edge of the wings and convects with the freestream flow. Here it is assumed that the induced flow does not significantly displace or deform the wake, which requires that the flight speed needs to be sufficiently large relative to the induced velocity. We assume a sinusoidal flapping motion, with equal upstroke and downstroke duration. The downstroke duration is known to vary between species [27, 28, 29] and with flight speed, , but is generally close to 50% [30, 31, 32, 33, 34, 35]. We leave the possible effects of varying downstroke time to future investigations. We used $N_U \times N_b = 41 \times 40$ points (flight direction and span direction) for the nodes of a triangular mesh (each triangle representing a vortex ring), with coordinates from 0 to U/f in flight direction and $-b/2$ to $b/2$ in span direction. Then a wing retraction transform was applied to the locations of the points. Birds and bats partially retract their wings during the upstroke [36]. In the current work wing retraction is modelled as

$$b = \begin{cases} b_{\max} & \tau < 0.5 \text{ (downstroke)} \\ b_{\min} + \frac{b_{\max} - b_{\min}}{2}\left(1 + \cos 4\pi\tau\right) & \tau \geq 0.5 \text{ (upstroke)} \end{cases}$$

Tab. 1: Sample ranges for thrust ratio T/L, reduced frequency k_f, flight speed U and lift production L/W.

	T/L	k_f	U (m/s)	L/W
min	0	1	3	0.2
max	0.3	6	20	3

with $b_{\min} = b_{\max} \cos\theta$. Here $b_{\max}$ is the maximum wingspan of the animal, θ the amplitude of the flapping motion and τ the normalized time variable running from 0 at the beginning of the downstroke, to 1 at the end of the upstroke. This transform ensures a smooth gradient from gliding flight with no upstroke wing retraction to large amplitude flapping flight with maximum wing retraction. Next the wake mesh was transformed by rotating the wing $\vartheta(\tau) = \theta \cos 2\pi\tau$ around the body axis. Note here that θ represents the maximum excursion from the centre, rather than the peak-to-peak amplitude often reported in studies of animal flight kinematics. A third transform tilts the stroke-plane an angle φ around the spanwise axis. Note that the angle φ is measured from the plane perpendicular to the flight direction, rather than the horizontal plane often reported in studies of animal flight kinematics (e.g. [37, 27, 29]), and that the angle is positive when the downstroke has a forward component (Figure 1).

A jackdaw (*Corvus monedula*) was chosen as a bird model, having a wingspan $b = 0.60$ m, a wing area $S = 0.059$ m^2 and a body mass of 0.180 kg[38]. The inviscid solution is characterized by reduced frequency and thrust ratio only, so the specific bird species has no influence on the optimisation. For the components due to zero-lift viscous drag, the solutions are non-dimensionalized as explained in section 3, thereby removing the influence of bird species. Only the lift dependent viscous drag could be affected by the choice of species, specifically as a function of the aspect ratio, as the optimal circulation distribution (equation 3) depends on the absolute chord length. However, this effect was found to be negligible (ESM S2, showing the sensitivity of the model to changes in $C_{Dv,2}/c$).

For a fixed stroke-plane angle the flapping amplitude θ was optimized for 200 randomized combinations of thrust ratio, reduced frequency, flight speed and lift production, over ranges specified in Table 1. A thrust ratio $T/L = 0$ corresponds to non-flapping flight, while $T/L = 0.3$ is about twice the maximum expected value at cruising speed as computed using the Pennycuick model for a database of 220 birds [4, (fig.13.11,p.370)]. From that same data, one could find that birds are expected to fly with a reduced frequency of 2 to 3 at the minimum power speed, so that the range $1 < k_f < 6$ covers a speed range from half the minimum power speed to twice the minimum power speed (assuming a constant flapping frequency). As the computations are performed in absolute dimensions, flight speed U was varied over a range plausible for the model bird, independent of reduced frequency. This forces variation in absolute flapping frequency. Finally the lift production is varied relative to the typical bird weight, so to cover scenarios in which the bird is carrying variable loads (e.g. fat stores or prey).

The wake geometry was optimized for minimal induced power, even though one would expect an animal to minimize total power. However, at lower speeds induced power will be dominant for most birds and bats. At high speeds, when viscous power components become dominant, the additional velocity component due to flapping will be relatively small for the expected wingbeat frequencies. With the effect on the viscous power components being small (see also figure 8) and induced power species independent, optimising for induced power will produce a more generally applicable model. For each optimisation an initial estimate for θ was used ($\theta = 45°$). In the second iteration the amplitude was increased by five degrees, and in the third an amplitude five degrees below the initial estimate was chosen. For the next iterations a quadratic polynomial was fitted to the three trials with the lowest power, of which the analytical minimum would serve as the next estimate. The search was limited to $0 < \theta < 90°$, the lower limit being non-flapping flight while at the upper limit the two wings touch at maximal excursion. The convergence tolerance was set to 1 degree. For each converged solution, the obtained amplitude θ and the resulting force components (D_{ind}, $D_{v,0}$ and $D_{v,2}$) and power components (P_{ind}, $P_{v,0}$ and $P_{v,2}$) were stored for analysis. The optimisation was repeated for different stroke-plane angles from 0° to 50° in steps of 10°, using the same 200 combinations of thrust ratio, weight support, reduced frequency, and flight speed.

3   Relating optimal flapping flight to non-flapping flight

The objective of this study is to characterize the effects of the reciprocating wings of flying animals, which we do by relating the optimized flapping wake data to their non-flapping equivalents (i.e. the limit $T/L = 0$).

The optimal flapping amplitude depends on the thrust ratio T/L and reduced frequency k_f. Then the expected dependency of the drag and power components on flapping amplitude can be substituted by a dependency on T/L and k_f. All the functions used for the non-linear regressions are based on observation of the data. This means that the relations fit the data very well, but they are not based on any formal derivations. The obtained relations should therefore be interpreted as interpolating functions applicable to forward flapping flight within the ranges of k_f and T/L specified in table 1. The approximating functions were fitted to the data using the NLINFIT() function from the statistics toolbox for Matlab R2013a (8.1.0.604), using bisquare robust fitting. For the drag and power components the robust fitting weights of each component were combined as $\hat{w} = (w_{D_{\mathrm{ind}}} \cdot w_{D_{v0}} \cdot w_{D_{v2}} \cdot w_{P_{\mathrm{ind}}} \cdot w_{P_{v0}} \cdot w_{P_{v2}})^{1/6}$ and the data refitted, so that each observation was treated equally for every component.

In the following section the optimized amplitude θ is expressed in terms of T/L, k_f and φ. In the second section, the derivation of the non-dimensionalized drag components is described and the approximating functions are explained, followed by a similar analysis for the power components. The last section shortly describes the effects of stroke-plane angle.

3.1   Optimized flapping amplitude

To our knowledge there is no known analytical relation between optimal flapping amplitude, thrust ratio and reduced frequency, so a function was designed to fit the data from the optimisation procedure (section 22.2). Flapping amplitude is limited to 90°. By using a tangent transform on the flapping amplitude, the transformed data can take any positive value. When we plot $\tan\theta$ for a single stroke-plane against thrust ratio T/L and reduced frequency k_f the data points are on a single surface, which corresponds to the previously made statement that the inviscid wake is characterized by these two variables. More specifically, $\tan\theta$ appears to be inversely proportional to the reduced frequency. Plotting $\tan\theta$ against T/Lk_f collapsed all data points onto a curve, which could be approximated by the function $\tan\theta = p_{1/2}\,(T/Lk_f)^{1/r} + p_1 T/Lk_f + p_4\,(T/Lk_f)^4$. Fitting the resulting model to the data then revealed that for higher reduced frequencies the actual amplitudes were under predicted. Allowing the function to produce amplitudes of more than 90°, resulted a better fit. This suggests that in certain conditions the predicted optimal amplitude are not physically possible, though those conditions are outside the parameter ranges of Table 1. The fitting model used is

$$\theta = (1 + qk_f)\arctan\left(p_{1/2}\left(\frac{T/L}{k_f}\right)^{\frac{1}{r}} + p_1\left(\frac{T/L}{k_f}\right) + p_4\left(\frac{T/L}{k_f}\right)^4\right). \tag{10}$$

To take into account the stroke-plane angle, the coefficients q, $p_{1/2}$, p_1 and p_4 were assumed to be quadratic polynomials of $\hat{\varphi} = \tan\varphi$: $p_i\,(\hat{\varphi}) = p_{i,0} + p_{i,1}\hat{\varphi} + p_{i,2}\hat{\varphi}^2$. The fitted coefficients of which the 95% confidence bounds deviate more than 10% from the estimate were removed, ($p_{1/2,1}$, $p_{1/2,2}$, $p_{1,2}$ and $p_{4,2}$), and the model was refitted. The removal of these coefficients narrowed the confidence bounds of the remaining coefficients and reduced the overall magnitude of the residuals. The final fitting coefficients are shown in Table 2. This fit approaches 95% of the data points to within the set convergence tolerance of 1 degree for the stroke amplitude optimisation. The remaining 5% of the data points are dominated by the highest stroke-plane angles ($\varphi = 50°$ has 66% of all residuals larger than 1 degree, $\varphi = 40°$ has 25%) and on average deviate 2.4 degrees from the fitted model. Figure 2 shows the fitted model as a function of reduced frequency and stroke-plane angle for different thrust ratios, indicating how increased thrust requirements require higher flapping amplitudes while increasing frequency allows for smaller amplitudes. Tilting the stroke-plane backward (increasing φ) requires larger stroke amplitudes, which intuitively makes sense as a compensation for the reduced vertical displacement of the wing in order to maintain thrust.
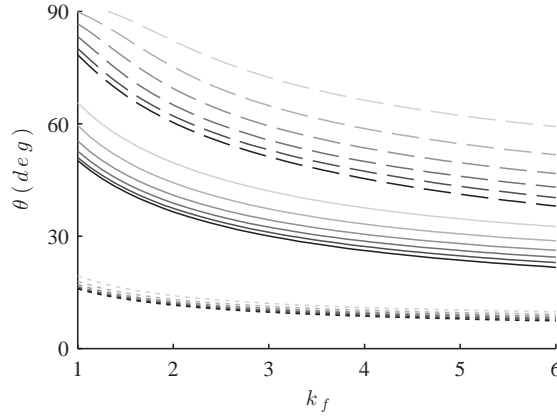
Fig. 2: Optimized stroke amplitude θ as a function of reduced frequency k_f, stroke-plane angle φ (from black $0°$ to grey $50°$), for thrust ratios $T/L = 0.01$ (dotted), $T/L = 0.1$ (solid) and $T/L = 0.3$ (dashed).

Tab. 2: Overview of the fitted coefficients for the wingbeat amplitude corresponding to equation 10 (mean $\pm$ 95% CI), with the rows indicating the quadratic polynomial coefficients for the model coefficient in each column. The empty places indicate coefficients not included in the final model.

	$p_{1/2}$	p_1	p_4	q	r
1	1.277 ± 0.048	6.214 ± 0.125	227.8 ± 12.7	0.0107 ± 0.0008	2.620 ± 0.047
$\hat{\varphi}$	-	-	-	0.0565 ± 0.0014	-
$\hat{\varphi}^2$	-	3.631 ± 0.082	1481 ± 42	-0.0169 ± 0.0011	-

3.2 Drag components and thrust

In the wake optimisation, induced drag D_{ind}, zero lift viscous drag $D_{\text{v},0}$ and lift dependent viscous drag $D_{\text{v},2}$ were computed (equations 7, 8 and 9). Each component has a corresponding expression for non-flapping flight (limit of $T/L = 0$). Induced drag is expressed as

$$D'_{\text{ind}} = \frac{L^2}{\pi b^2 \left(\frac{1}{2}\rho U^2\right)}, \tag{11}$$

which is a familiar expression from fixed wing aerodynamics for an ideally loaded planar wing. The non-dimensionalized induced drag data was then approximated with

$$\frac{D_{\text{ind}}}{D'_{\text{ind}}} = 1 + \left(p_0 \frac{1}{k_f} + p_1\right) \frac{T}{L}. \tag{12}$$

The non-flapping solution for zero lift drag is $D'_{\text{v},0} = \frac{1}{2}\rho U^2 \int_{-b/2}^{b/2} c C_{D\text{v},0} dy$ (with $C_{D,\text{v},0}$ from equation 4). For the wing shape described by equation 5 expression evaluates to approximately

$$D'_{\text{v},0} = 1.33\rho\sqrt{\nu U^3 bS}. \tag{13}$$

The zero lift data could be described by the function

$$\frac{D_{\text{v},0}}{D'_{\text{v},0}} = 1 + \left(p_0^{D_{v0}} + p_1^{D_{v0}} k_f + p_2^{D_{v0}} \frac{1}{k_f^2}\right) \frac{T}{L}. \tag{14}$$

The non-flapping solution for lift dependent viscous drag can be expressed as $D'_{\text{v},2} = \frac{1}{2}\rho U^2 \int_{-b/2}^{b/2} c C_{D\text{v},2} C_\ell^2 dy$, which evaluates to approximately $D'_{\text{v},2} = 2C_{D\text{v},2} L^2/\rho U^2 S$. Note here the similarity to induced drag

$$D'_{\text{v},2} = C_{D\text{v},2} \pi AR D'_{\text{ind}}, \tag{15}$$

Tab. 3: Fitted coefficients for the drag components corresponding to equations 12, 14 and 16, with polynomial coefficients as defined by equation 17 (mean $\pm$ 95% CI). The empty places indicate coefficients not included in the final model.

	D_{ind}	$D_{\text{v},0}$	$D_{\text{v},2}$
$p_{0,0}$	9.250 ± 0.026	-0.590 ± 0.017	9.298 ± 0.041
$p_{0,1}$	-	-	-
$p_{0,2}$	2.931 ± 0.058	-1.145 ± 0.015	1.301 ± 0.058
$p_{1,0}$		0.239 ± 0.004	-0.659 ± 0.016
$p_{1,1}$	-1.969 ± 0.022	0.197 ± 0.005	-1.521 ± 0.023
$p_{1,2}$	-	0.446 ± 0.006	-
$p_{2,0}$	n.a.	-0.715 ± 0.038	n.a.

with $AR = b^2/S$ being the aspect ratio. Because of the similarity to induced drag, the approximating model is similar to equation 12,

$$\frac{D_{\text{v},2}}{D'_{\text{v},2}} = 1 + \left(p_0^{D_{v2}} \frac{1}{k_f} + p_1^{D_{v2}} \right) \frac{T}{L}. \tag{16}$$

Now all drag components are expressed as $\frac{D}{D'} = 1 + f_D(k_f) \frac{T}{L}$, which results in good fits for each separate stroke-plane angle. As only f_D changes with stroke-plane angle, it can be expressed as

$$f_D(k_f, \varphi) = \left(\frac{D}{D'} - 1 \right) \frac{L}{T}.$$

Assuming the coefficients p_0 and p_1 are quadratic functions of $\hat{\varphi} = \tan \varphi$,

$$p_i(\hat{\varphi}) = p_{i,0} + p_{i,1}\hat{\varphi} + p_{i,2}\hat{\varphi}^2, \tag{17}$$

the model for each drag component now has 6 coefficients to fit to the simulated data points. As with the procedure for the stroke amplitude, we removed the polynomial coefficients with low confidence. The fitted coefficients for each component are shown in Table 3 and the fitted functions $f_D(k_f, \varphi)$ are visualized in figure 3.

The animal flaps its wings with the purpose of generating thrust, which in steady forward flight has to counter aerodynamic drag. The total drag on an animal can be expressed as the sum of the body drag and the drag on the wings, so that the thrust required for steady flight is $T = D_{\text{body}} + D_{\text{ind}} + D_{\text{v},0} + D_{\text{v},2}$. With the approximations introduced above, equations 12, 14 and 16, all being linear functions of thrust, the following equation for the required thrust ratio is found,

$$\frac{T}{L} = \frac{D'_{\text{v},0} + (1 + C_{D\text{v},2}\pi AR) D'_{\text{ind}} + D_{\text{body}}}{L - f_{D_{\text{v},0}}(k_f, \varphi) D'_{\text{v},0} - \left(f_{D_{\text{ind}}}(k_f, \varphi) + f_{D_{\text{v},2}}(k_f, \varphi) C_{D\text{v},2}\pi AR \right) D'_{\text{ind}}}. \tag{18}$$

The numerator is the total drag for non-flapping flight, while the effects on the required thrust due to flapping are in the denominator.

3.3 Power components

In steady flight models the required aerodynamic power is obtained by multiplying the drag with the flight speed, $P = DU$. However, to find the aerodynamic power for flapping flight it is not sufficient to multiply the required thrust found from equation 18 with the flight speed, because this thrust is only the wingbeat averaged force along the direction of flight. Within the wingbeat work is also done perpendicular to this direction. Therefore, in a similar manner as with the drag components, we non-dimensionalized the power components by their non-flapping equivalents, and examined their relation to reduced frequency and thrust ratio.

The general behaviour of the non-dimensionalized power components is very similar to their
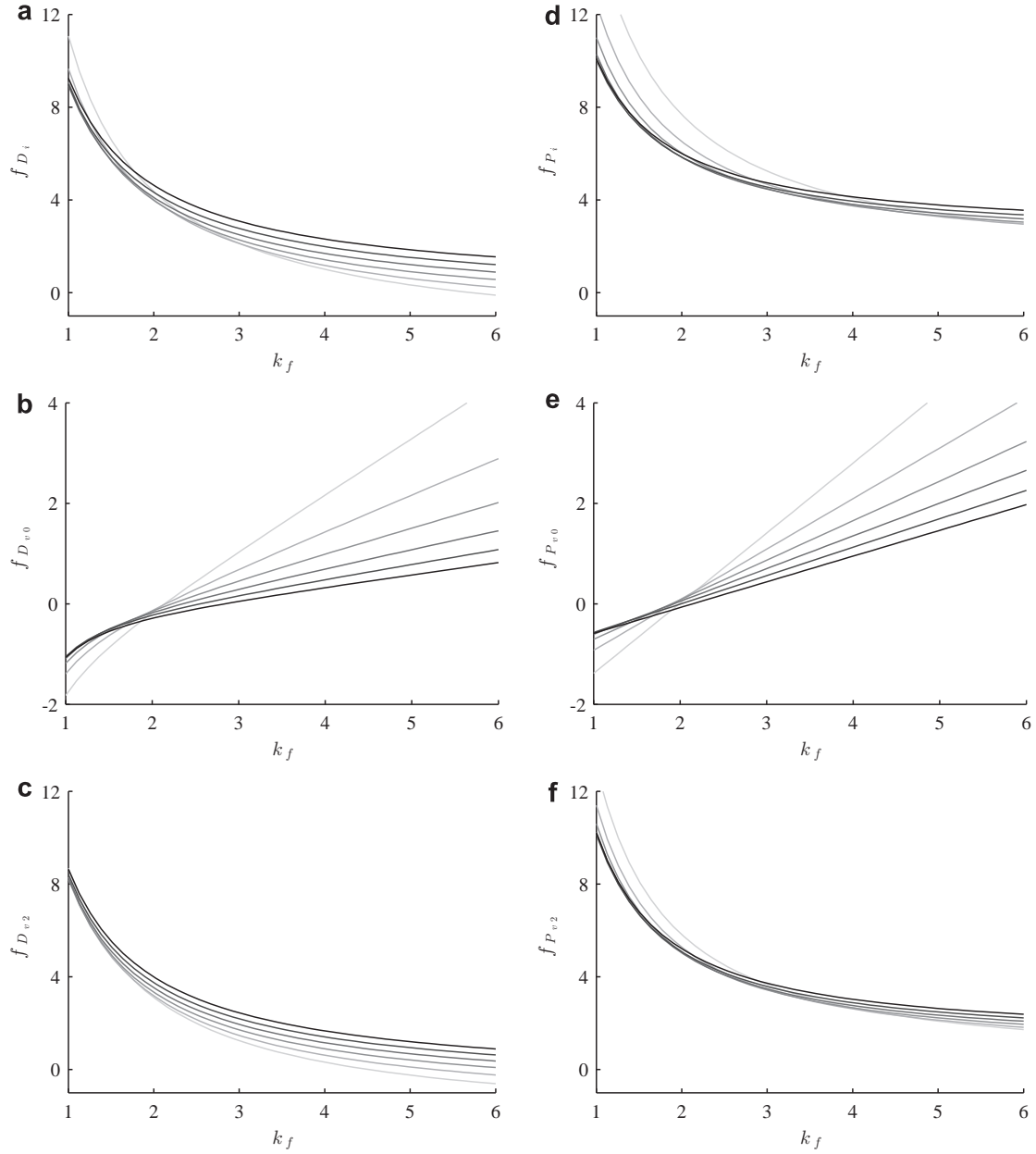
Fig. 3: Fitted models $f_D(k_f, \varphi) = \left(\frac{D}{D'} - 1\right)\frac{L}{T}$ for (a) induced drag (eq. 12), (b) zero lift viscous drag (eq. 14), (c) lift dependent viscous drag (eq. 16), (d) induced power (eq. 19), (e) zero lift power (eq. 20), (f) and lift dependent viscous power (eq. 21). The six lines represent the stroke-plane angles φ 0 (black line) to $50°$ (lightest shade of grey).

Tab. 4: Fitted coefficients for the power components corresponding to equations 19, 20 and 21, with polynomial coefficients as defined by equation 17 (Mean ± 95% CI).

	P_{ind}	$P_{\mathrm{v},0}$	$P_{\mathrm{v},2}$
$p_{0,0}$	7.517 ± 0.078	-1.101 ± 0.014	8.851 ± 0.065
$p_{0,1}$	-	-	-
$p_{0,2}$	4.913 ± 0.128	-1.183 ± 0.022	2.807 ± 0.099
$p_{1,0}$	2.573 ± 0.058	0.512 ± 0.004	1.354 ± 0.050
$p_{1,1}$	-1.259 ± 0.048	0.227 ± 0.007	-0.943 ± 0.033
$p_{1,2}$	-	0.431 ± 0.008	-
$p_{2,0}$	n.a.	-	n.a.
r	1.135 ± 0.025	n.a.	1.201 ± 0.022

drag counterparts, so that similar models can be used

$$\frac{P_{\mathrm{ind}}}{P'_{\mathrm{ind}}} \;=\; 1 + \left(p_0 \frac{1}{k_f^r} + p_1 \right) \frac{T}{L}, \tag{19}$$

$$\frac{P_{v,0}}{P'_{v,0}} \;=\; 1 + \left(p_0 + p_1 k_f + p_2 \frac{1}{k_f^2} \right) \frac{T}{L}, \tag{20}$$

$$\frac{P_{v,2}}{P'_{v,2}} \;=\; 1 + \left(p_0 \frac{1}{k_f^r} + p_1 \right) \frac{T}{L}. \tag{21}$$

Note here that equations 19 and 21 have an additional power coefficient r, which notably improved the fit for low reduced frequencies. Again only the factor in front of the thrust ratio is a function of stroke-plane angle and reduced frequency

$$f_P \left(k_f, \varphi \right) = \left(\frac{P}{P'} - 1 \right) \frac{L}{T}.$$

The coefficients p_0 and p_1 are again modelled as quadratic polynomials of $\hat{\varphi} = \tan \varphi$. The fitted coefficients are given in Table 4 and the fitted functions f_P are visualized in figure 3. For all components it seems that f_D is less than f_P, i.e. that the penalty due to flapping is more severe on the power than on the drag.

Equation 18 can be used in equations 19, 20 and 21, which combine with $P_{\mathrm{body}} = D_{\mathrm{body}} U$ to total aerodynamic power

$$\frac{P_{\mathrm{tot}}}{P'_{\mathrm{tot}}} = \left(\frac{P_{\mathrm{ind}}}{P'_{\mathrm{ind}}} \right) \frac{D'_{\mathrm{ind}}}{T'} + \left(\frac{P_{v,0}}{P'_{v,0}} \right) \frac{D'_{v,0}}{T'} + \left(\frac{P_{v,2}}{P'_{v,2}} \right) \frac{D'_{v,2}}{T'} + \frac{D_{\mathrm{body}}}{T'}. \tag{22}$$

Here the total power is non-dimensionalized by the non-flapping total power. Every term (P/P') is a function of reduced frequency k_f, stroke-plane angle φ and thrust ratio T/L. Of these, T/L is itself a function of k_f, φ, and the non-flapping drag components D'. Note that the reciprocal of equation 22 is equivalent to the definition of propulsive efficiency commonly used as a performance measure for the propulsion system of fixed wing aircraft, i.e.

$$\begin{aligned} \eta \;&=\; TU/P \\ &=\; \frac{P'_{\mathrm{tot}}}{P_{\mathrm{tot}}}. \end{aligned}$$

3.4 Optimising stroke-plane angle

Equation 22 is a function of the non-flapping drag components and two kinematic parameters: stroke-plane angle φ and the flapping frequency in the form of reduced frequency k_f. From figure 3 it can be observed that the stroke-plane angle affects lift dependent components different from
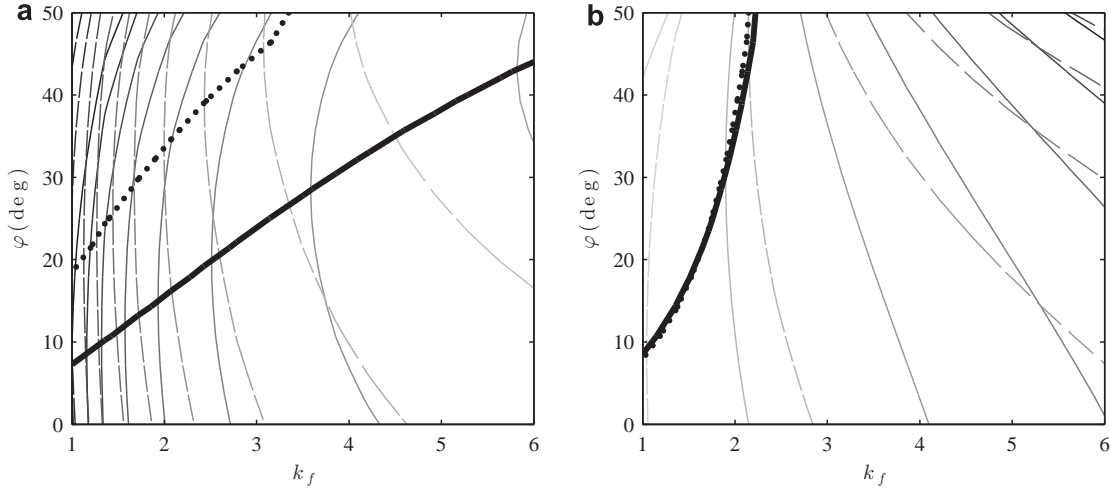
Fig. 4: (a) optimal stroke-plane angle across reduced frequencies, for minimal induced drag (thick dashed line) and minimal induced power (thick solid line). Thin lines indicate isolines of $f_{D_{\text{ind}}}$ (dashed) and $f_{P_{\text{ind}}}$ (solid), decreasing with reduced frequency k_f. (b) In case of pure zero lift drag, there is no functional minimum within the explored parameter range. Instead, the thick lines indicate the stroke-plane angles with maximum zero lift drag (dashed) and zero lift power (solid). Thin lines indicate isolines of $f_{D_{v0}}$ (dashed) and $f_{P_{v0}}$ (solid), increasing with reduced frequency.

the lift independent components. Figure 4a illustrates the optimal stroke-plane angle ($\mathrm{d}f_D/\mathrm{d}\varphi = 0$ and $\mathrm{d}f_P/\mathrm{d}\varphi = 0$) in the case where induced drag is dominant, $D'_{\text{ind}} \gg D'_{v0}, D'_{v2}$, as a function of reduced frequency. For a constant flapping frequency, reduced frequency is inversely proportional to the flight speed, so the lower the speed, the more horizontal becomes the stroke-plane.

On the other hand, when the zero lift drag component is dominant, $D'_{v0} \gg D'_{\text{ind}}, D'_{v2}$, figure 4b shows only a maximum for $\mathrm{d}f_D/\mathrm{d}\varphi = 0$ and $\mathrm{d}f_P/\mathrm{d}\varphi = 0$ within the range of $0 \leq \varphi \leq 50°$. This plot implies tilting the stroke-plane forward ($\varphi < 0$) allows for lower values of $f_{D_{v0}}$ and $f_{P_{v0}}$. Even though the non-lift producing case, which this limit implies, has not been simulated, intuitively the tendency towards a forward tilted stroke-plane makes sense, considering its similarity to breaststroke swimming (i.e. drag based thrust).

A flying bird or bat will be between these limiting cases, so at this stage one can only argue that the actual optimal stroke-plane angle for any species will be less than that required for minimising induced drag (dashed line in figure 4a). Finding the specific optimal stroke-plane angle requires evaluating the relative contributions of each non-flapping drag component, which will differ across species.

4   Jackdaw example

To illustrate the implications of equations 12 to 16 and 19 to 21, again the jackdaw is used [38]. We start with determining the non-flapping drag components, the sum of which determines the base level of thrust that needs to be produced, as depicted in figure 5. These drag components are then used in equation 22 and 18. For a given flight speed and frequency the stroke-plane angle can now be optimized. In figure 6 this is done for the jackdaw flying with a wingbeat frequency of 6.4 Hz, which is a reference frequency derived from the allometric relation $f_{\text{ref}} = m^{3/8}g^{1/2}b^{-23/24}S^{-1/3}\rho^{-3/8}$ [39, 4]. The optimal stroke-plane angle gets more horizontal for low flight speeds, which corresponds with observations of slow flying animals [27, 35]. Here it should be noted that this horizontal orientation in this model is not because it increases the angle of attack of the wings, but purely related to increasing the horizontal component of the airflow over the wings. At high flight speeds the optimal stroke-plane angle is approximately vertical. For speeds above 17 m/s an actual optimum ($\mathrm{d}\eta/\mathrm{d}\varphi = 0$) does not exist for positive φ, but considering the large separation between the contours of equal efficiency, the penalty for using any other stroke-plane angle is very small.

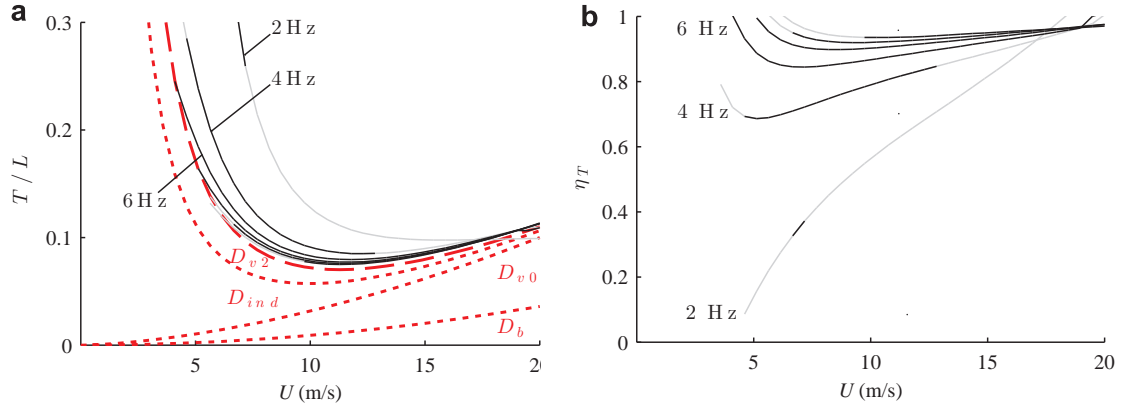In section 2 it was also noted that the model is only applicable to fast forward flight. In

Fig. 5: (a) Thrust ratio for a jackdaw over a range of speeds computed from equation 18 with the stroke-plane angle optimized for minimum power (equation 22). The grey lines indicate extrapolated data. The thick dashed line (red online) represents the non-flapping thrust requirement. The regions between the dotted lines (red online) indicate the contributions of the different drag components. (b) Thrust efficiency, non-flapping thrust divided by flapping thrust $\eta_T = T'/T$, indicating how thrust efficiency increases with wingbeat frequency and with flight speed.

helicopter theory the lower limit is often set to twice the induced velocity in hover [40]. In the current model this limit is in most cases implicitly enforced by the upper limit on thrust ratio. The induced velocity is related to induced drag by $v_i/V = D_{\mathrm{ind}}/L$. From Glauert's interpolation of induced velocity for slow flight one can derive

$$\frac{v_i}{v_{\mathrm{ih}}} = \left(\left(\frac{1}{4} \left(\frac{V}{v_{\mathrm{ih}}} \right)^4 + 1 \right)^{1/2} - \frac{1}{2} \left(\frac{V}{v_{\mathrm{ih}}} \right)^2 \right)^{1/2},$$

where v_{ih} is the induced velocity in hover [41]. This means that at $V/v_{\mathrm{ih}} = 2$ the induced drag to lift ratio is $D_{\mathrm{ind}}/L \approx 0.24$. When adding profile drag it is very unlikely that the required thrust ratio will remain below 0.3 at this low speed, so that the assumption of fast forward flight is implicitly justified by the upper limit on thrust ratio.

As indicated by equation 18, the drag will be slightly increased due to the flapping of the wings. For a range of flapping frequencies, figure 5 shows the extent of this increase. Focussing on frequencies above the reference frequency of 6.4 Hz, it appears the deviations from the non-flapping thrust requirement are minor. The effects are more clear when looking at the thrust efficiency, which for the reference frequency is lowest around 0.85. For higher frequencies it seems the efficiency is almost speed independent with a value around 95%. Another interesting observation from these plots is the behaviour at low speeds. The thrust efficiency seems to increase above unity, which at first might seem wrong. However, the efficiency is taken relative to the non-flapping case. In slow flight, with a tilted stroke-plane, the beating of the wing temporarily increases the airspeed over the wing, which reduces the induced drag. If then during the recovery stroke, less lift is produced, also here there will be less induced drag, compared to the non-flapping situation.

Figure 7 shows propulsive efficiency, $\eta_P = T'U/P$, visualized for a range of wingbeat frequencies, together with the corresponding optimized stroke-plane angles and wingbeat amplitudes. Higher wingbeat frequencies generally increase efficiency, but the relative gain in efficiency decreases with increasing frequency. Also, the relative benefit of higher frequency decreases with increasing flight speed. Figure 7 also shows how high propulsive efficiency is related to lower wingbeat amplitudes. However, here it should be kept in mind that this concerns the optimized amplitude, i.e. reducing the amplitude without changing frequency and stroke-plane angle will inevitably result in a lower efficiency.

Considering again the reference wingbeat frequency of 6.4 Hz, the jackdaw flies with a propulsive efficiency of 80% around 10 m/s increasing to over 90% for speeds above 15 m/s. In this range the optimal wingbeat amplitude would be around 35 degrees. At 10 m/s the stroke-plane angle
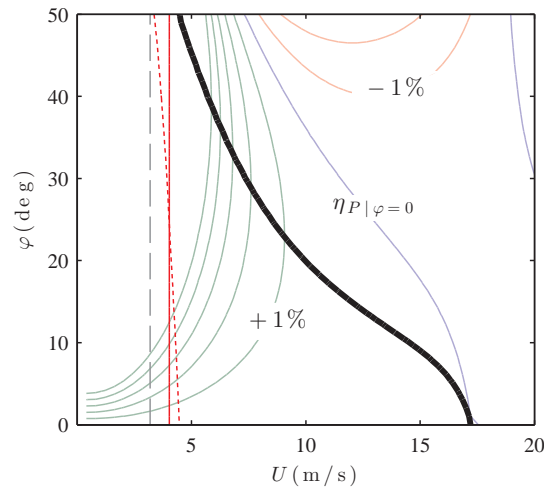
Fig. 6: Stroke-plane angle minimising total power over a range of flight speeds for a jackdaw (thick black line), with a wingbeat frequency of 6.4 Hz. Thin contours indicate the relative difference to the vertical stroke-plane, $\eta_P (U, \varphi) - \eta_{P|\varphi=0} (U)$, in steps of 1%. Low speed limits are indicated: minimum simulated thrust ratio $T/L > 0.3$ (dotted) and maximum simulated reduced frequency $k_f > 6$ (solid). Dashed line indicates the speed that is twice the induced velocity in hover.
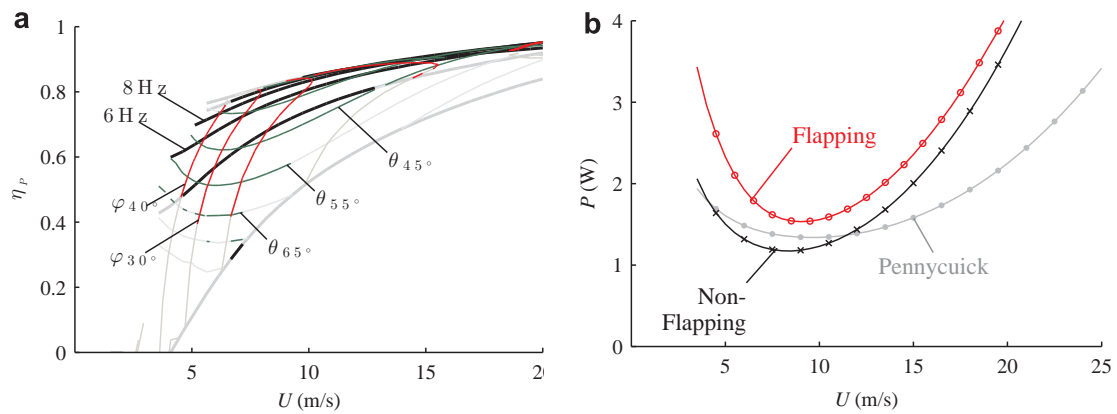
Fig. 7: Example of flapping flight performance for a jackdaw. (a) Propulsive efficiency ($\eta_p = T^{'}U/P$) as a function of flight speed optimized for a range of frequencies (thick lines) from 2 to 15 Hz. Thin contour lines indicate corresponding optimal flapping amplitudes θ (online in green) and stroke-plane angles φ (online in red). Lighter grey lines indicate extrapolation outside sampled range. (b) Power curve for the same jackdaw, with a wingbeat frequency of 6.4 Hz (open circles, online in red). Non-flapping curve is also shown (crosses). As a reference the power curve computed with Pennycuick's model Flight 1.25 (grey) is included.

would be tilted 20 degrees from vertical and tilted more vertical for higher speeds. The power curve corresponding to this frequency is shown in figure 7b. Also the non-flapping power curve is shown, illustrating how the flapping increases the power requirement. The speed dependency of the propulsive efficiency causes the speed for minimum power to increase compared to the non-flapping curve.

For reference the power curve as computed by Flight 1.25 (Pennycuick's model) is also shown. Below the minimum power speed, Pennycuick's model is between the flapping and the non-flapping curve. At higher speeds it predicts much lower power requirements. A notable effect of this is the higher maximum range speed (minimal P/U). Both the non-flapping and the flapping curve predict much lower maximum range speeds. This might be related to concerns raised by field observations where birds generally fly slower than expected [7]. Field observations of jackdaw flight speeds (A. Hedenström and S. Åkesson 2014, unpublished data) indicate a preferred flight speed between 11.6 m/s and 14.3 m/s (95% confidence interval for the corrected mean observed flight speed) for level flying individual birds (ESM S3). For this specific bird the Pennycuick model predicts a maximum range speed of 15.9 m/s, which is outside of this confidence interval, while the model we developed in this work predicts this characteristic speed at 12.1 m/s, which is well within the observed range.

As a final consideration, the effect of flapping can be examined for each power component separately. Figure 8 shows the power factors $(P_{\text{ind}}/P'_{\text{ind}})$, $(P_{\text{v},0}/P'_{\text{v},0})$ and $(P_{\text{v},2}/P'_{\text{v},2})$ from equation 22. The induced power factor, which in the Pennycuick model is denoted by the symbol k, has been a subject of debate. Early estimates of this parameter were in the range of 1.1 to 1.2, commonly used for helicopters. Recently a value as low as 0.9 has been suggested, to match the Pennycuick model with field observations [7]. As can be observed from figure 8, all of these estimates might be very optimistic, as for the jackdaw reference frequency the induced power factor never goes below 1.4. Even for the extremely high wingbeat frequency of 15 Hz the parameter only approaches the previous worst case estimate of 1.2. In figure 8d-f the contribution due to flapping is shown relative to the total non-flapping power. This shows that around the minimum power speed the reference frequency of 6.4 Hz would result in roughly 30% increase of aerodynamic power solely due to the increased induced power, demonstrating the importance of estimating this parameter correctly. The zero lift power factor increases strongly for decreasing speed. This is a result of the normalisation with the non-flapping power component that is very small, while the flapping wings are experiencing a higher level of viscous drag. Looking at the relative contribution due to flapping (Figure 8e), it follows that the effects of flapping on the zero lift power are relatively small. This supports the arguments in section 22.2 for optimising induced power only. The lift dependent viscous power factor is very similar in behaviour to the inviscid induced power factor, though slightly lower. The relative effect on the total power curve is less than half that of the induced power factor, which makes sense considering that for this bird the non-flapping lift dependent viscous power is approximately 57% of the induced power (equation 15).

5   Concluding remarks

We developed a model for the aerodynamic cost of vertebrate flight that incorporates the main effects of flapping wings. For a range of combinations of thrust ratio, reduced frequency and stroke-plane angle, the wingbeat amplitude θ was optimized for minimum power, using a numerical vortex wake model. The results were converted into an explicit general model, represented by equation 22. Our model provides potential explanations to divergence between the model that is commonly used to estimate flight power in flying vertebrates [5, 4] and observations [7].

The Hall and Hall model [12] computes the energetically most efficient distribution of circulation for a given wake geometry. This results in an ideal solution, equivalent to that for fixed wing lifting line theory. In all subsequent computations it is assumed that a bird or bat wing will be able to produce this ideal wake. However, it may occur that the wake prescribes a lift coefficient that is not physically attainable for the aerofoil. Additionally, when the required lift coefficient would be realistic for the aerofoil, it may still require a geometric angle that is not within the range of motions of the wing. Figure 9a-c show the distribution of lift coefficient along the span throughout the wingbeat at three different speeds: 5 m/s, 10 m/s and 15 m/s, estimated for the example of a jackdaw of section 4 (see S4 for details). At 5 m/s large lift coefficients are prescribed for
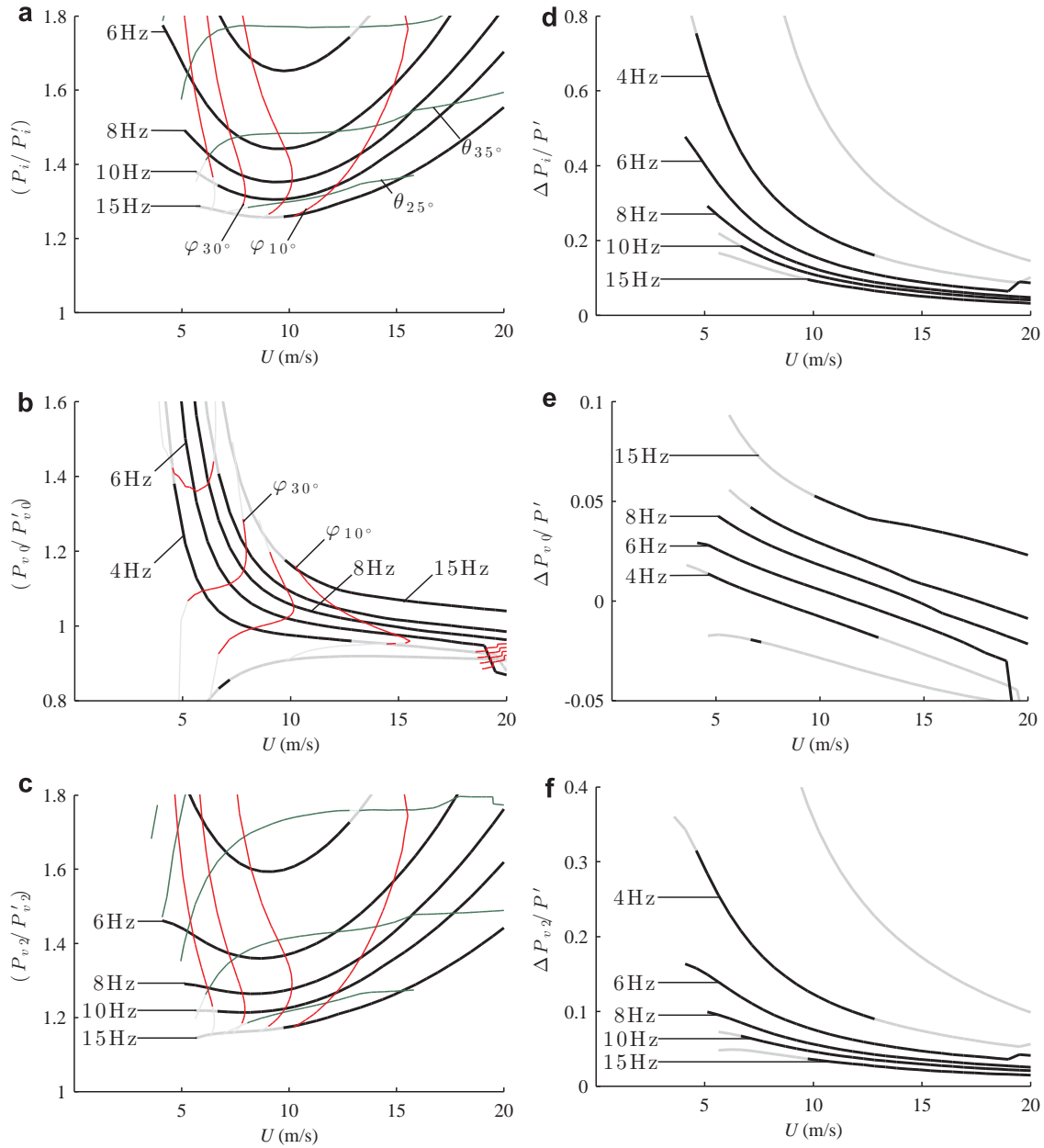
Fig. 8: Per power component effect of flapping for a jackdaw. Frames (a), (b) and (c) show the factor the corresponding non-flapping power component has to be multiplied with to include the effects of flapping, e.g. the top left frame shows the induced power factor. (online version in colour) Frames (e), (f) and (g) show the effect of each component relative to the total non-flapping power curve, i.e. the $\Delta P/P'$, indicating the importance of including flapping.

the body region and the inner wing, exceeding the maximum lift coefficient for many aerofoils (though unsteady mechanisms could increase the maximum lift coefficient [42]). This suggests the bird may not be able to produce this optimal load distribution and it has to resort to alternative distributions, which inevitably has to result in increased induced power. However, the model does not take into account the additional lifting tail surface, usually maximally spread in slow flight, which would reduce the required lift coefficient at the inner wing. To achieve the prescribed lift distribution along the wing at this low speed a considerable amount of wing twist is required, as illustrated in figure 9d, but bird wings are flexible and wing tip reversal is not uncommon among birds at low speeds [43]. Around the minimum power speed (10 m/s) the maximum lift coefficient is below the stall value of most aerofoils and the range of required wing twist is reduced (figure 9b,e). This trend is continued with increasing speed (figure 9c,f).
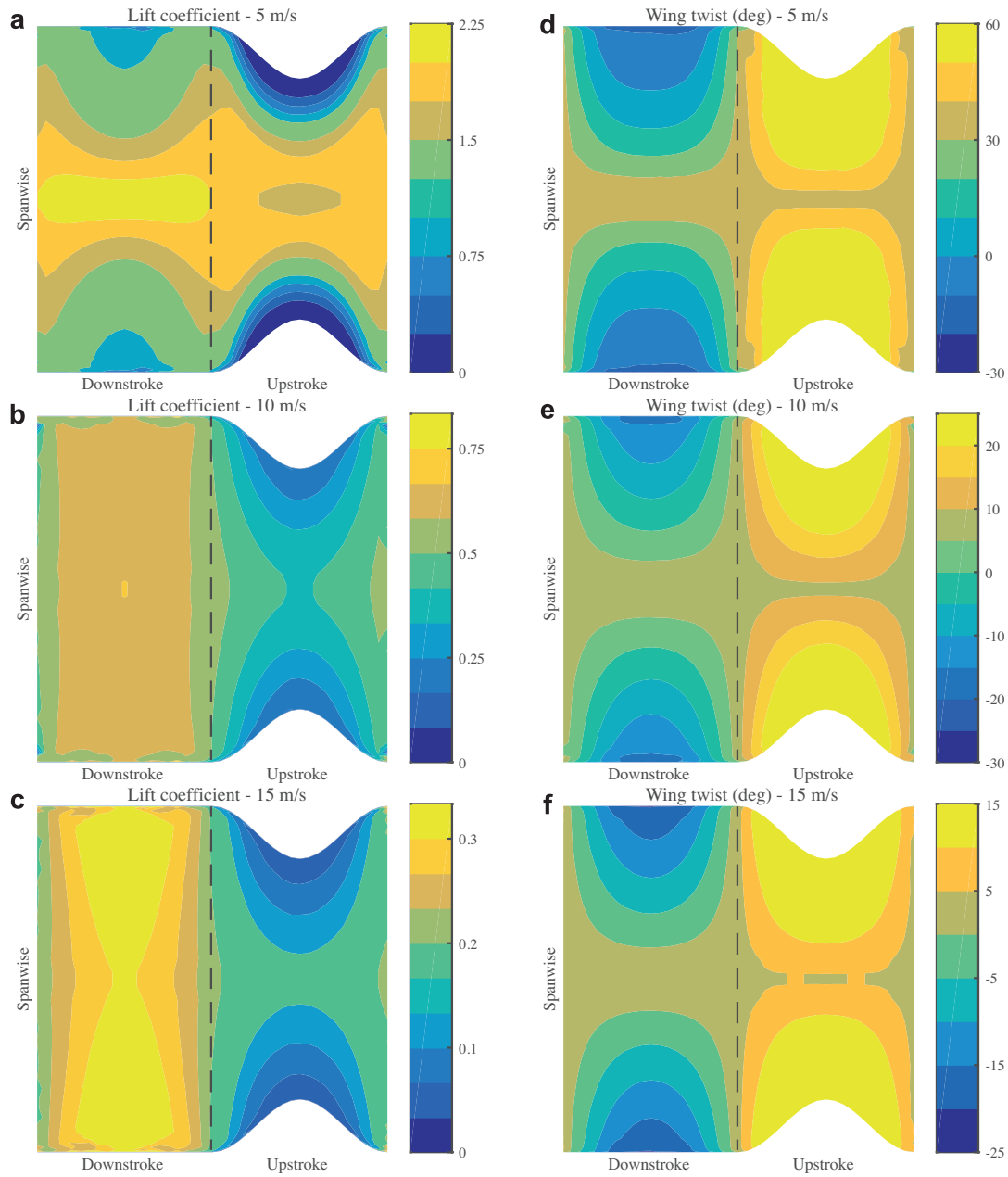
Fig. 9: Lift coefficients (left column) and wing twist (right column) relative to the flight path for the jackdaw example.

On a similar note the effect of wake roll-up has not been taken into account. Even before the

wake leaves the wing it starts to roll-up into the tip vortices, which could alter the realized lift distribution. Fixed wing aircraft frequently use wing tip devices, which are designed to improve the efficiency of the wing [44]. The separated outer primaries of bird wings have been suggested to serve a similar purpose [45, 46, 47]. In fixed wing aerodynamics, these deviations are dealt with by introducing a span efficiency factor. A similar factor should be expected for flapping flight, though its value could be much more variable compared to its fixed wing equivalent. A consideration in future models could thus be to quantify these effects in real animals and include them in the model.

Author contributions   M.K. conceived of the study, performed the computations and analysis, and drafted the manuscript.. L.C.J and A.H. contributed to the design of the study, interpreting the data and drafting the manuscript. All authors gave final approval for publication.

Conflict of interests   We have no competing interests.

References

[1] Hedenström A, Alerstam T. 1995 Optimal Flight Speed of Birds. *Philos. Trans. R. Soc. B Biol. Sci.* **348**, 471–487. (doi:10.1098/rstb.1995.0082).

[2] Hedenström A, Alerstam T. 1996 Skylark optimal flight speeds for flying nowhere and somewhere. *Behav. Ecol.* **7**, 121–126.

[3] Grodzinski U, Spiegel O, Korine C, Holderied MW. 2009 Context-dependent flight speed: evidence for energetically optimal flight speed in the bat *Pipistrellus kuhlii*? *J. Anim. Ecol.* **78**, 540–548. (doi:10.1111/j.1365-2656.2009.01526.x).

[4] Pennycuick, CJ. 2008 *Modelling the flying bird*. Amsterdam, The Netherlands: Elsevier.

[5] Pennycuick, CJ. 1968 Power requirements for horizontal flight in the pigeon *Columba livia. J. Exp. Biol.* **49**, 527–555.

[6] Hedenström A, Liechti F. 2001 Field estimates of body drag coefficient on the basis of dives in passerine birds. *J. Exp. Biol.* **204**, 1167–1175.

[7] Pennycuick, CJ, Åkesson S, Hedenström A. 2013 Air speeds of migrating birds observed by ornithodolite and compared with predictions from flight theory. *J. R. Soc. Interface* **10**, 20130419. (doi:10.1098/rsif.2013.0419).

[8] Pennycuick CJ, Klaassen M, Kvist A, Lindström Å. 1996 Wingbeat frequency and the body drag anomaly: wind-tunnel observations on a thrush nightingale (*Luscinia luscinia*) and a teal (*Anas crecca*). *J. Exp. Biol.* **199**, 2757–2765.

[9] Parslew B, Crowther WJ. 2010 Simulating avian wingbeat kinematics. *J. Biomech.* **43**, 3191–3198. (doi:10.1016/j.jbiomech.2010.07.024).

[10] Rayner JMV. 1979 A vortex theory of animal flight. Part 2. The forward flight of birds. *J. Fluid Mech.* **91**, 731–763. (doi:10.1017/S0022112079000422).

[11] Phlips PJ, East RA, Pratt NH. 1981 An unsteady lifting line theory of flapping wings with application to the forward flight of birds. *J. Fluid Mech.* **112**, 97–125. (doi:10.1017/S0022112081000311).

[12] Hall KC, Hall SR. 1996 Minimum induced power requirements for flapping flight. *J. Fluid Mech.* **323**, 285–315.

[13] Spedding GR. 2003 A family of vortex wakes generated by a thrush nightingale in free flight in a wind tunnel over its entire natural range of flight speeds. *J. Exp. Biol.* **206**, 2313–2344. (doi:10.1242/jeb.00423).

[14] Anderson JD Jr. 2007 *Fundamentals of Aerodynamics*. McGraw-Hill Education, 4th edition.

[15] Salehipour H, Willis DJ. 2013 A coupled kinematics-energetics model for predicting energy efficient flapping flight. *J. Theor. Biol.* **318**, 173–196. (doi:10.1016/j.jtbi.2012.10.008).

[16] Hall KC, Pigott SA, Hall SR. 1997 AIAA 97-0827 Power Requirements for Large-Amplitude Flapping Flight. In *35th Aerosp. Sci. Meet. Exhibition, Reno, NV, 6–9 January*. Reston, VA: AIAA.

[17] Pennycuick CJ. 1968 A wind-tunnel study of gliding flight in the pigeon *Columba livia. J. Exp. Biol.* **49**, 509–526.

[18] Tucker VA, Parrott GC. 1970 Aerodynamics of gliding flight in a falcon and other birds. *J. Exp. Biol.* **52**, 345–367.

[19] Pennycuick CJ. 1971 Gliding flight of the white-backed vulture *Gyps africanus. J. Exp. Biol.* **55**, 13–38.

[20] Tucker VA, Heine C. 1990 Aerodynamics of gliding flight in a Harris' Hawk, *Parbuteo unicinctus. J. Exp. Biol.* **149**, 469–489.

[21] Pennycuick CJ. 1971 Gliding flight of the dog-faced bat *Rousettus aegyptiacus* observed in a wind tunnel. *J. Exp. Biol.* **55**, 833–845.

[22] Withers PC. 1981 An aerodynamic analysis of bird wings as fixed aerofoils. *J. Exp. Biol.* **90**, 143–162.

[23] Pennycuick CJ, Heine CE, Kirkpatrick SJ, Fuller MR. 1992 The profile drag of a hawk's wing, measured by wake sampling in a wind tunnel. *J. Exp. Biol.* **165**, 1–19.

[24] Lentink D, Müller UK, Stamhuis E, De Kat R, Van Gestel W, Veldhuis LLM, Henningsson P, Hedenström A, Videler JJ, Van Leeuwen JL. 2007 How swifts control their glide performance with morphing wings. *Nature* **446**, 1082–1085. (doi:10.1038/nature05733).

[25] Kruyt JW, Quicazán-Rubio EM, Van Heijst GF, Altshuler DL, Lentink D. 2014 Hummingbird wing efficacy depends on aspect ratio and compares with helicopter rotors. *J. R. Soc. Interface* **11**. (doi:10.1098/rsif.2014.0585).

[26] Blasius H. 1908 Grenzschichten in Flüssigkeiten mit kleiner Reibung. *Zeitschrift für Math. und Phys.* **56**, 1–37.

[27] Tobalske BW, Dial KP. 1996 Flight kinematics of black-billed magpies and pigeons over a wide range of speeds. *J. Exp. Biol.* **199**, 263–280.

[28] Hedrick TL, Tobalske BW, Biewener AA. 2003 How cockatiels (*Nymphicus hollandicus*) modulate pectoralis power output across flight speeds. *J. Exp. Biol.* **206**, 1363–1378. (doi:10.1242/jeb.00272).

[29] Rosén M, Hedenström A, Spedding GR. 2007 Wake structure and wingbeat kinematics of a house-martin *Delichon urbica. J. R. Soc. Interface* **4**, 659–668. (doi:10.1098/rsif.2007.0215).

[30] Park KJ, Rosén M, Hedenström A. 2001 Flight kinematics of the barn swallow (*Hirundo rustica*) over a wide range of speeds in a wind tunnel. *J. Exp. Biol.* **204**, 2741–50.

[31] Rosén M, Spedding GR, Hedenström A. 2004 The relationship between wingbeat kinematics and vortex wake of a thrush nightingale. *J. Exp. Biol.* **207**, 4255–68. (doi:10.1242/jeb.01283).

[32] Hedenström A, Rosén M, Spedding GR. 2006 Vortex wakes generated by robins *Erithacus rubecula* during free flight in a wind tunnel. *J. R. Soc. Interface* **3**, 263–76. (doi:10.1098/rsif.2005.0091).

[33] Henningsson P, Spedding GR, Hedenström A. 2008 Vortex wake and flight kinematics of a swift in cruising flight in a wind tunnel. *J. Exp. Biol.* **211**, 717–30. (doi:10.1242/jeb.012146).

[34] Wolf, M, Johansson LC, Von Busse R, Winter Y, Hedenström A. 2010 Kinematics of flight and the relationship to the vortex wake of a Pallas' long tongued bat (*Glossophaga soricina*). *J. Exp. Biol.* **213**, 2142–53. (doi:10.1242/jeb.029777).

[35] Von Busse R, Hedenström A, Winter Y, Johansson LC. 2012 Kinematics and wing shape across flight speed in the bat, *Leptonycteris yerbabuenae. Biol. Open* **1**, 1226–38. (doi:10.1242/bio.20122964).

[36] Tobalske BW, Warrick DR, Clark CJ, Powers DR, Hedrick TL, Hyder GA, Biewener AA. 2007 Three-dimensional kinematics of hummingbird flight. *J. Exp. Biol.* **210**, 2368–82. (doi:10.1242/jeb.005686).

[37] Dudley R, Ellington CP. 1990 Mechanics of forward flight in bumblebees I. Kinematics and morphology. *J. Exp. Biol.* **148**, 19–52.

[38] Rosén, M. & Hedenström, A., 2001 Gliding flight in a jackdaw: a wind tunnel study. *J. Exp. Biol.* **204**, 1153–66.

[39] Pennycuick CJ. 1996 Wingbeat frequency of birds in steady cruising flight: new data and improved predictions. *J. Exp. Biol.* **199**, 1613–1618.

[40] Seddon J. 1990 *Basic helicopter aerodynamics.* Oxford: BSP Professional Books.

[41] Glauert H. 1926 *A general theory of the autogyro.* ARC Reports & Memoranda no. 1111. Cranfield, UK: Aeronautical Research Council.

[42] Muijres FT, Johansson LC, Hedenström A. 2012 Ledge vortex in a slow-flying passerine. *Biol. Lett.* **8**, 554–557. (doi:10.1098/rsbl.2012.0130).

[43] Tobalske BW, Hedrick TL, Biewener AA. 2003 Wing kinematics of avian flight across speeds. *J. Avian Biol.* **34**, 177–184. (doi:10.1034/j.1600-048X.2003.03006.x)

[44] Kroo I. 2001 Drag due to lift: Concepts for Prediction. *Annu. Rev. Fluid Mech.* **33**, 587–617. (doi:10.1146/annurev.fluid.33.1.587).

[45] Tucker VA. 1993 Gliding birds: reduction of induced drag by wing tip slots between the primary feathers. *J. Exp. Biol.* **180**, 285-310.

[46] Tucker VA. 1995 Drag reduction by wing tip slots in a gliding Harris' hawk, *Parabuteo unicinctus. J. Exp. Biol.* **198**, 775–781.

[47] Berens M. 2008 *Potential of Multi-Winglet Systems to Improve Aircraft Performance.* Diplom-ingenieur, Technischen Universität Berlin.